83.5 dB Dynamic Range Lead-Free SWIR Image Sensors Based on Monolithic Fabrication of InAs Thin-Film Quantum Dot Photodiodes

Myonglae Chu, Wenya Song, Joo Hyoung Kim, Tristan Weydts, Vladimir Pejovic, Minhyun Jin, Sang Yeon Lee, Yoora Seo, Jonas Bentell, Abu Bakar Siddik, Isabel Pintor Monroy, Marina Vildanova, Arman Uz Zaman, Tae Jin Yoo, Antonia Malainou, Wagdy Hussein, Annachiara Spagnolo, Gauri Karve, Itai Lieberman, and Pawel E. Malinowski

imec, Kapeldreef 75, 3001 Leuven, Belgium
E-mail: Myonglae.chu@imec.be

***Abstract*—This paper proposes a scalable SWIR sensor using monolithic thin-film photodiodes (TFPD) and introduces a lead-free SWIR image sensor based on InAs quantum dots (QD) to comply with material restrictions. The InAs QDPD is fabricated on a silicon readout wafer with a 3T pixel structure, enabling dual conversion gain for enhanced dynamic range. Experimental results demonstrate external quantum efficiencies of 28% at 1200 nm and 4.8% at 1400 nm, with a dynamic range of 83.5 dB. The proposed sensor exhibits reduced noise levels and no visible random telegraph signal (RTS) noise by the frame based correlated double sampling (CDS).**

***Keywords*—CMOS Image Sensor, InAs, Quantum dot (QD) photodiode, Short-wavelength infrared (SWIR) sensor**

I. Introduction

The demand for image sensors in the short-wavelength infrared (SWIR) range (1000 nm to 2000 nm) has been steadily increasing due to their superior sensitivity compared to silicon photodiodes for specific use cases in medical imaging, security, automotive, and industrial inspection. These applications benefit from the enhanced detection capabilities of SWIR sensors, which can provide clearer images and more accurate data in challenging environments.

However, traditional SWIR image sensors, which often rely on wafer-to-wafer bonding to connect III-V photodiode arrays to silicon readout circuits [1], face challenges related to scaling and fabrication costs due to their complicated bonding processes. The wafer-to-wafer bonding process is not only complex but also expensive, making it difficult to produce these sensors at a large scale. Additionally, the alignment and bonding of wafers can introduce defects and reduce the overall yield, further increasing the cost.

To address these challenges, we propose a SWIR sensor that utilizes monolithic fabrication of thin-film photodiodes (TFPD). This approach offers several advantages, including improved scalability, reduced manufacturing complexity, and the potential for new form factors. By integrating the photodiodes directly onto the silicon readout wafer, it eliminates the need for wafer-to-wafer bonding, simplifying the fabrication process and enhancing the sensor's reliability [2]. This monolithic integration not only reduces the number of processing steps but also minimizes the risk of misalignment and defects, leading to higher yields and lower costs. Furthermore, this work introduces a lead-free SWIR image sensor based on indium arsenide (InAs) quantum dots (QD) [3] to comply with material restrictions.

This InAs QD-based sensor shows tunable optical properties, which can be precisely controlled by adjusting QD size and composition, optimizing the sensor's target wavelength. The ability to fine-tune the peak wavelength allows for customization of the sensor for specific applications, enhancing its performance. In addition, due to the monolithic fabrication of TFPD on the top of silicon, it can achieve a high dynamic range (DR) because it allows the use of the silicon area to implement a dual conversion gain (DCG) capacitor and an extra switch within the limited pixel area. The dual conversion gain mechanism enables the sensor to handle a wide range of light intensities, improving its performance in both low-light and high-light conditions.

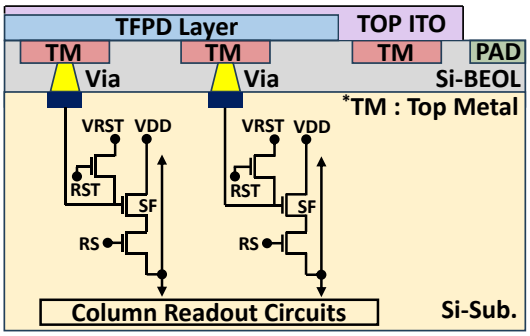

Fig. 1. The simplified sensor architecture of InAs QDPD on silicon readout circuit.

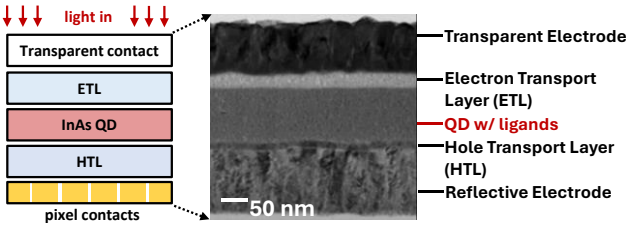

Fig. 2. Stack structure of InAs QD pixel and X-TEM image of a PD stack with 1-step coated SPLE InAs QD.

II. Quantum Dot Photodiode and Image Sensor Design

Fig. 1 shows a simplified schematic of the sensor architecture. The InAs quantum dot photodiode (QDPD) is fabricated on top of a silicon readout wafer, featuring a 3T pixel structure. The QDPD layer is implemented using a spin coating process, applied layer by layer. This method ensures uniform deposition and optimal performance of the QDPD layer. The TFPD, through the top metal (TM), is connected

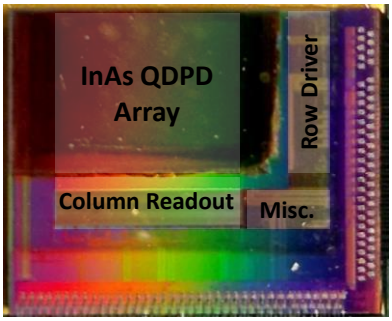

Fig. 3. The micrograph of the prototype sensor.

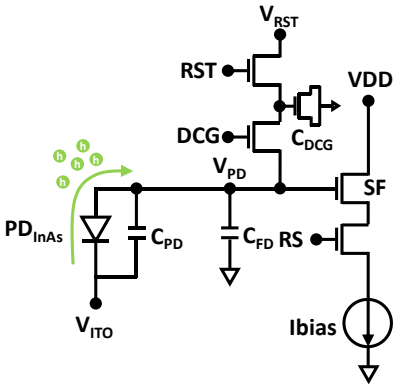

Fig. 4. The pixel model of hole type InAs QDPD with pixel transistors.

to the source follower at the individual pixel level, thereby forming the pixel array.

Fig. 2 illustrates the more details of InAs QDPD stack structure along with a cross-TEM image, providing a detailed view of the layer composition and interfaces. Depending on the arrangement of the charge transport layers, the type of signal charge (either hole or electron) can vary, which impacts the sensor's performance characteristics. To minimize the junction leakage of the reset transistor (RST), which contributes to dark current, this paper employs a hole collection readout circuit (h2ROIC), allowing for a low reset voltage of V_{PD}. This approach effectively reduces the dark current of the junction, enhancing the overall image quality.

The micrograph of the prototype chip is presented in Fig. 3, showcasing the physical layout and integration of the sensor components. Fig. 4 provides a detailed electrical equivalent model of the pixel for the hole-type 3T-pixel, illustrating the circuit elements and their interactions. Essentially, the TFPD sensor does not require a photodiode area in silicon, freeing up this area for other purposes. This available space can be utilized for various enhancements, such as a pixel-level sample and hold circuit for global shutter operation, a pixel-level analog-to-digital converter, or, in this case, a dual conversion gain to increase the dynamic range (DR) and to be used as a pixel analog gain.

The high conversion gain (HCG) for a 5 µm pixel size is primarily achieved by the InAs QDPD, which has a capacitance of approximately 20 fF. The low conversion gain (LCG), which is 108 fF, is defined as the sum of the HCG and the capacitance of the dual conversion gain (C_{DCG}). For the hole-type pixel operation, the pixel uses a 1.8V V_{RST} as the initial reset level for the photodiode (V_{PD}) and sets the V_{ITO} voltage to 5V for the cathode of PD_{InAs}. This configuration

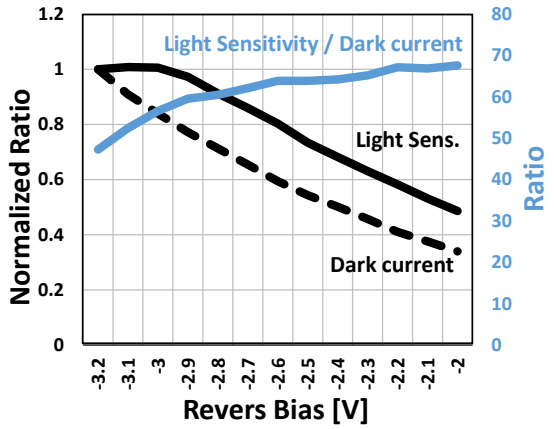

Fig. 5. Measured light sensitivity change, dark current changes and sensitivity over dark ratio with bias voltage.

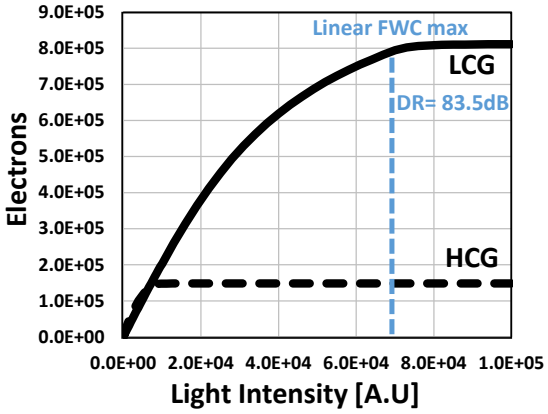

Fig. 6. Measured photon response curve of InAs QDPD DCG pixel.

ensures optimal performance and maximizes the dynamic range of the sensor.

III. Test Restuls

To observe the linearity of photodiode sensitivity and dark current as V_{PD} increases with the incoming photons, Fig. 5 shows the normalized change ratios of each parameter, as well as the ratio of light sensitivity to dark current. The results indicate that InAs QDPD sensitivity and dark current decrease with a reduction in PD_{InAs} reverse bias; however, the ratio of these parameters increases. This characteristic leads to linearity degradation but simultaneously helps to enhance the dynamic range, like logarithmic pixel [4].

Fig. 6 shows the photon response curve, with an achievable dynamic range of 83.5 dB. The linear full well capacity (FWC) of HCG and LCG is 71.9 ke- and 782 ke-, respectively. This wide dynamic range is crucial for capturing detailed images in varying light conditions, making the sensor suitable for applications requiring high sensitivity and accuracy.

The noise characteristics of this sensor is illustrated in Fig. 7 using the inverse cumulative distribution function (ICDF). To improve noise performance, this sensor employs frame CDS with a 1.3 µs time interval, effectively reducing reset KTC noise, which is the dominant dark noise source in 3T pixels, as well as random telegraph signal (RTS) noise. Fig. 7a clearly show that the thermal noise value improved from

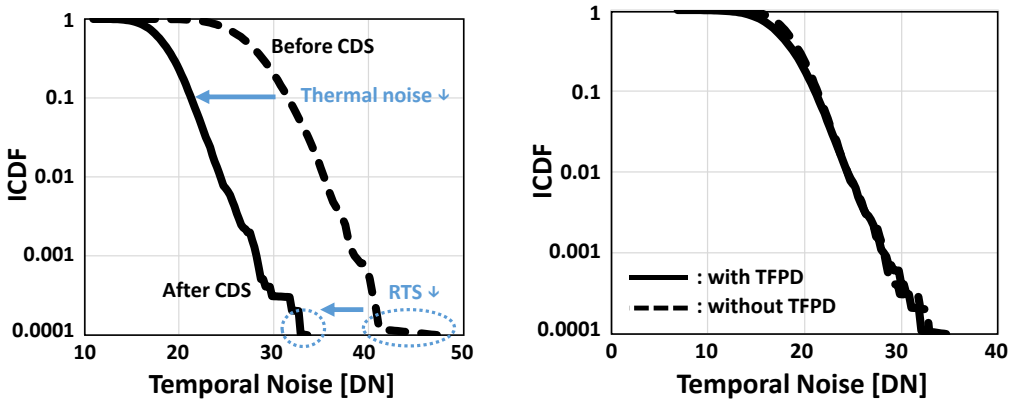

(a) (b)

Fig. 7. (a) Inverse cumulative distribution function (ICDF) before and after CDS; and (b) RTS performances comparison with and without InAs QDPD (CDS time: 1.3 µs).

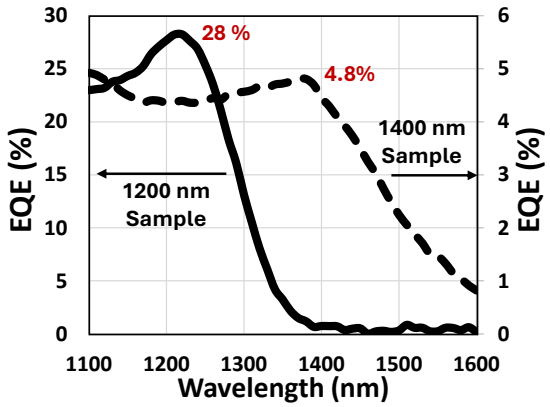

Fig. 8. Measured EQE of two different stacks (for peak EQE @ 1200 and 1400 nm) versus wavelength.

Parameter	Value	Unit
Technology	130	[µm]
Pixel Size / Resolution	5 / 0.39	[µm] / MP
Dark Current (DC) (1200 / 1400 nm, @ -3.2V)	23.6 / 80	[µA/cm^2]
Dark Read Noise (HCG / LCG)	52.2 / 276	[e-]
Conversion Gain (HCG / LCG)	8.13 / 1.48	[µV/e-]
FWC (HCG / LCG)	71.9k / 782k	[e-]
PRNU (1200 / 1400 nm)	8.1 / 3.5	[%]
Dynamic Range (HCG / DCG)	67 / 83.5	[dB]

Table. 1. Measured Image Sensor Performance. Except for DC and PRNU, all results are from the 1200 nm samples.

32 digital numbers (DN) to 21, and the ICDF tail showing RTS noise is also improved. The noise comparison with and without PD_{InAs} is also studied (Fig. 7b). Despite the general knowledge that QDPDs have numerous traps which can be seen as RTS noise, the proposed pixel exhibits no visible RTS noise from the InAs QDPD, and the overall RTS noise level is lower than that of the source follower RTS noise level. This is why there is no difference in the ICDF tail with and without PD_{InAs}.

The experimental results demonstrate external quantum efficiencies (EQE) of 28% at 1200 nm and 4.8% at 1400 nm for two fabricated stacks, as illustrated in Fig. 8. Additionally, Fig. 8 shows the wavelength tunability of Quantum Dot Photodetectors (QDPD). Generally, QDPDs can detect different wavelengths, ranging from visible light to shortwave infrared, depending on their size. However, when fabricating QDPDs with the same structure to detect longer wavelengths, several issues arise, such as an increase in dark current and a decrease in EQE. These issues are caused by the reduction in band gap caused by the larger quantum dot size and the increase in charge traps resulting from a lower ratio of stable crystal planes. Table 1 summarizes the sensor performance metrics.

The captured sample images, shown in Fig. 9, illustrate the advantages of SWIR images compared to RGB images. From our test setup, we captured images both without and with smoke. In the first case, without smoke, the SWIR sensor can distinguish different materials even if their colors are the same. In the second case, with smoke, the SWIR sensor can see objects through the smoke. Figure 10 demonstrates that the 1200 SWIR sensor is capable of detecting objects through a silicon wafer. Table 2 provides a performance comparison with other SWIR pixels [1,5-8].

IV. Conclusions

These proof-of-concept imagers demonstrate an encouraging path towards Quantum Dot (QD) Short-Wave Infrared (SWIR) breakthroughs in higher volume applications. The experimental results highlight the significant potential of InAs Quantum Dot Photodiodes (QDPDs) in achieving high external quantum efficiencies (EQE) and dynamic range, while addressing challenges such as dark current and sensitivity degradation. The integration of noise reduction techniques, including frame CDS and hole collection readout circuits, has effectively minimized reset KTC noise and random telegraph signal (RTS) noise, thereby enhancing overall image quality. Furthermore, the ability of SWIR sensors to penetrate smoke and distinguish materials regardless of color underscores their potential for applications in various fields, such as surveillance, environmental monitoring, and industrial inspection. These advantages make SWIR sensors a valuable tool for enhancing visibility and detection capabilities in challenging conditions. The findings presented in this paper guide the reader through

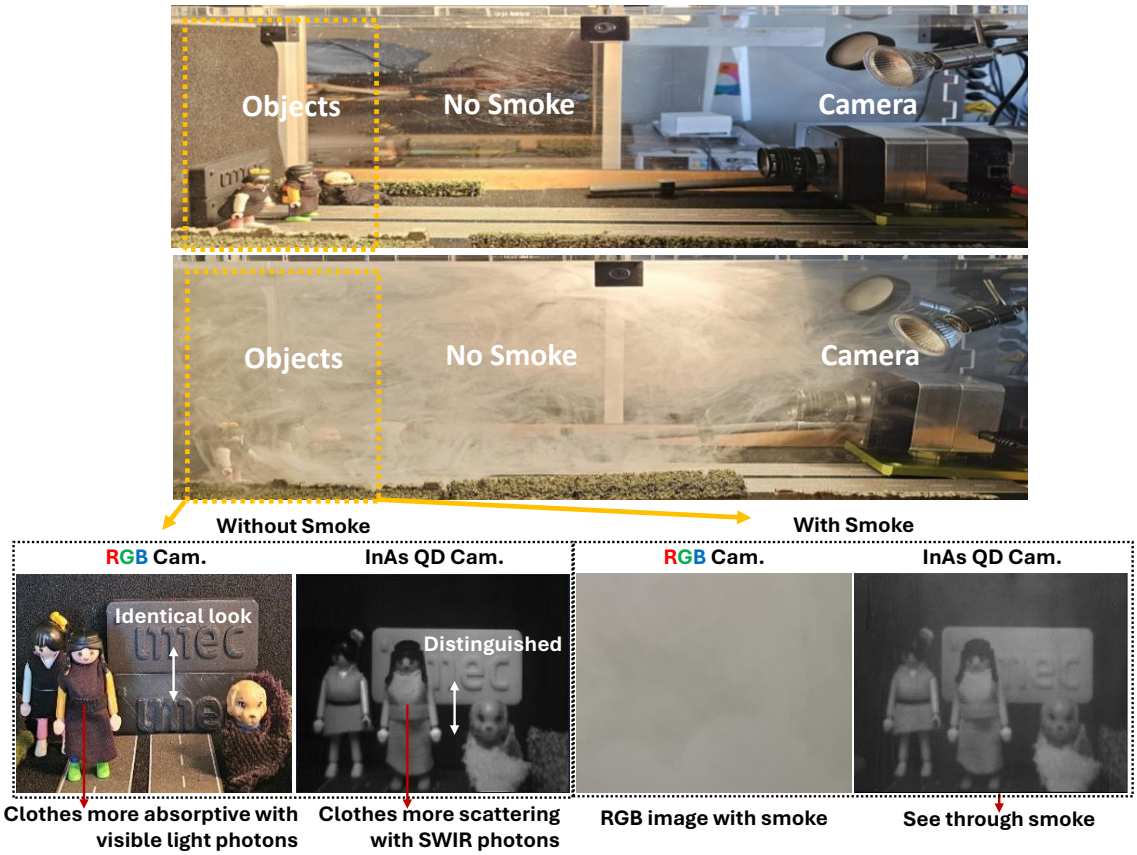

Fig. 9. RGB and 1200nm wavelength Sample Images captured w/ and w/o smoke condition.

Parameter	This work[1)]		[1]	[5]	[6]	[7]	[8][2)]	
Photodiode	InAs QD		InGaAs	PbS QD	PbS QD	Ge-on-Si	InAs QD	
Pixel Pitch [μm]	5		5	7	1.62 /2.2	10	-	
Spectral range [nm]	400 – 1600		400-1700	400-1700	1400	850-1400	400-1600	
Stack (peak λ)	1200	1400	-				940	1400
Dark current [uA/cm^2]	23.6	80	*0.0025	< 0.005	**0.3 / 0.51	-	*0.02	*100
Peak EQE [%]	28	4.8	-	15 - 45	*60	-	*39	*15
PRNU [%]	8.1	3.5	-	-	1.4 / 0.7	-	-	-

**Values read from the graph, **Recalculated values from the data, [1)] Results with -3.2 V bias voltage ,[2)] Results with -1.5 V bias voltage.*

Table. 2. Pixel performance comparison table.

the promising capabilities of QDPDs, paving the way for future advancements in sensor technology and their deployment in high-resolution imaging and sensing applications.

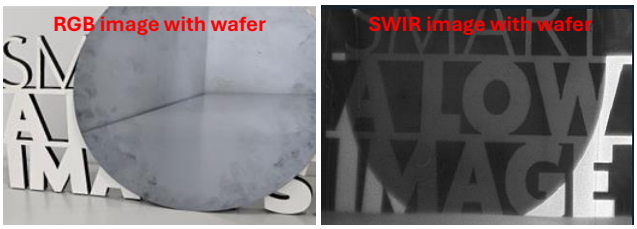

Fig. 10. RGB and 1200nm wavelength Sample Images captured w/ and w/o silicon wafer.

REFERENCES

[1] S. Manda et al., "High-definition visible-SWIR InGaAs image sensor using Cu-Cu bonding of III-V to silicon wafer," *IEDM 2019*, pp. 16-7.

[2] E. Georgitzikis et al., "Organic- and QD-based image sensors integrated on 0.13 μm CMOS ROIC for high-resolution, multispectral infrared imaging," *IISW 2019*, pp. R43.

[3] W. Song et al., "Lead-free quantum dot photodiodes for next-generation short-wave infrared optical sensors," *IEDM 2024*, pp. 41-8.

[4] M. Bae et al., "A Linear-Logarithmic CMOS Image Sensor with Adjustable Dynamic Range," *IEEE Sensors Journal*, vol. 15, no. 6, pp. 3456-3463, June 2015.

[5] C. Gregory et al., "Bandwidth and thermal stability of colloidal quantum dot sensors," *SPIE 2022*, vol. 12107.

[6] J. S. Steckel, "1.62μm global shutter quantum dot image sensor optimized for near and shortwave infrared," *IEDM 2021*, pp. 23-4.

[7] C.-L. Chen et al., "Advancements in solid-state circuits," *ISSCC 2020*, pp. 5-3.

[8] O. Enoki et al., "Lead-free colloidal InAs quantum dot image sensor for infrared applications," *IEDM 2024*, pp. 41-7.